Convective injection into stratospheric intrusions

Cameron R. Homeyer,[1] Kenneth P. Bowman,[1] Laura L. Pan,[2] Mark A. Zondlo,[3] and James F. Bresch[2]

Received 15 August 2011; revised 16 September 2011; accepted 3 October 2011; published 10 December 2011.

[1] Stratospheric intrusions (tropopause folds) are known to be major contributors to stratosphere-troposphere exchange. The specific mixing processes that lead to irreversible exchange between stratospheric intrusions and the surrounding troposphere, however, are not entirely understood. This study presents direct observations of moist convection penetrating into stratospheric intrusions. The characteristics of convective injection are shown by using in situ aircraft measurements, radar reflectivities, and model analyses. Convective injection is observed at altitudes up to 5 km above the bottom of a stratospheric intrusion. Aircraft measurements from the Stratosphere-Troposphere Analyses of Regional Transport 2008 (START08) experiment show that convective injection in stratospheric intrusions can be uniquely identified by coincident observations of water vapor greater than about 100 ppmv and ozone greater than about 125 ppbv. Trajectory analyses show that convective injection can impact transport in both directions: from troposphere to stratosphere and from stratosphere to troposphere. We present a conceptual model of the synoptic meteorological conditions conducive to convective injection in stratospheric intrusions. In particular, convective injection is found to be associated with a "split front" where the upper-level frontal boundary outruns the surface cold front.

Citation: Homeyer, C. R., K. P. Bowman, L. L. Pan, M. A. Zondlo, and J. F. Bresch (2011), Convective injection into stratospheric intrusions, *J. Geophys. Res.*, *116*, D23304, doi:10.1029/2011JD016724.

1. Introduction

[2] The occurrence and impact of stratospheric intrusions in the upper troposphere and lower stratosphere (UTLS) has been the focus of many previous stratosphere-troposphere exchange (STE) studies and aircraft experiments [e.g., *Reed*, 1955; *Danielsen*, 1968; *Shapiro*, 1980; *Shapiro et al.*, 1987; *Browell et al.*, 1987; *Cooper et al.*, 2004; *Appenzeller and Davies*, 1992; *Appenzeller et al.*, 1996; *Flentje et al.*, 2005; *Pan et al.*, 2007, 2010]. Stratospheric intrusions (or tropopause folds) are one of the key mechanisms of STE and have a significant influence on the composition of the UTLS, which in turn affects chemistry, climate, and the radiation budget [e.g., *Hoskins*, 1991; *Holton et al.*, 1995; *Stohl et al.*, 2003]. There are several known processes that lead to irreversible exchange (mixing) of air between stratospheric intrusions and the surrounding troposphere during their lifecycles. Several of these are collectively referred to as clear air turbulence [e.g., *Shapiro*, 1976, 1978, 1980]. Mechanisms for generation of clear air turbulence include inertio-gravity waves [e.g., *Danielsen et al.*, 1991], Kelvin-Helmholtz instabilities [e.g., *Shapiro*, 1980] and boundary layer mixing [e.g., *Johnson and Viezee*, 1981]. Diabatic processes such as latent heating and radiative cooling associated with clouds near the tropopause can also be important [e.g., *Price and Vaughan*, 1993; *Lamarque and Hess*, 1994]. Filamentation and roll-up of intrusions into vortices that interleave tropospheric and stratospheric air masses is a significant mixing process [e.g., *Appenzeller et al.*, 1996]. Convection is also a potential source of irreversible mixing during stratospheric intrusions. The impacts of convective injection could be large given the deep descent of intrusions into the troposphere and the ability of convection to rapidly transport air vertically. Convective injection of tropospheric air into stratospheric intrusions has been inferred from observations, but has not been observed directly [e.g., *Langford and Reid*, 1998; *Reid and Vaughan*, 2004; *Cooper et al.*, 2005].

[3] Stratospheric intrusions occur outside of the tropics, and they have distinct climatological characteristics in terms of their depth and seasonality. The frequency of stratospheric intrusions has been found to be highest along the subtropical jet stream and the magnitude of stratosphere-to-troposphere transport in general is larger in middle latitudes and during the winter and spring seasons [e.g., *Waugh and Polvani*, 2000; *Seo and Bowman*, 2001; *Olsen et al.*, 2002; *Wernli and Bourqui*, 2002; *Sprenger and Wernli*, 2003; *Sprenger et al.*, 2003]. Although they are more common in the subtropics, individual stratospheric intrusions tend to be deeper (descend to lower altitudes) and have stronger mass exchange fluxes along the polar jet stream in midlatitudes [e.g., *Wernli and Bourqui*, 2002; *Sprenger et al.*, 2003]. *Sprenger and Wernli* [2003] show that the deepest exchange

[1]Department of Atmospheric Sciences, Texas A&M University, College Station, Texas, USA.
[2]National Center for Atmospheric Research, Boulder, Colorado, USA.
[3]Department of Civil and Environmental Engineering, Princeton University, Princeton, New Jersey, USA.

0148-0227/11/2011JD016724

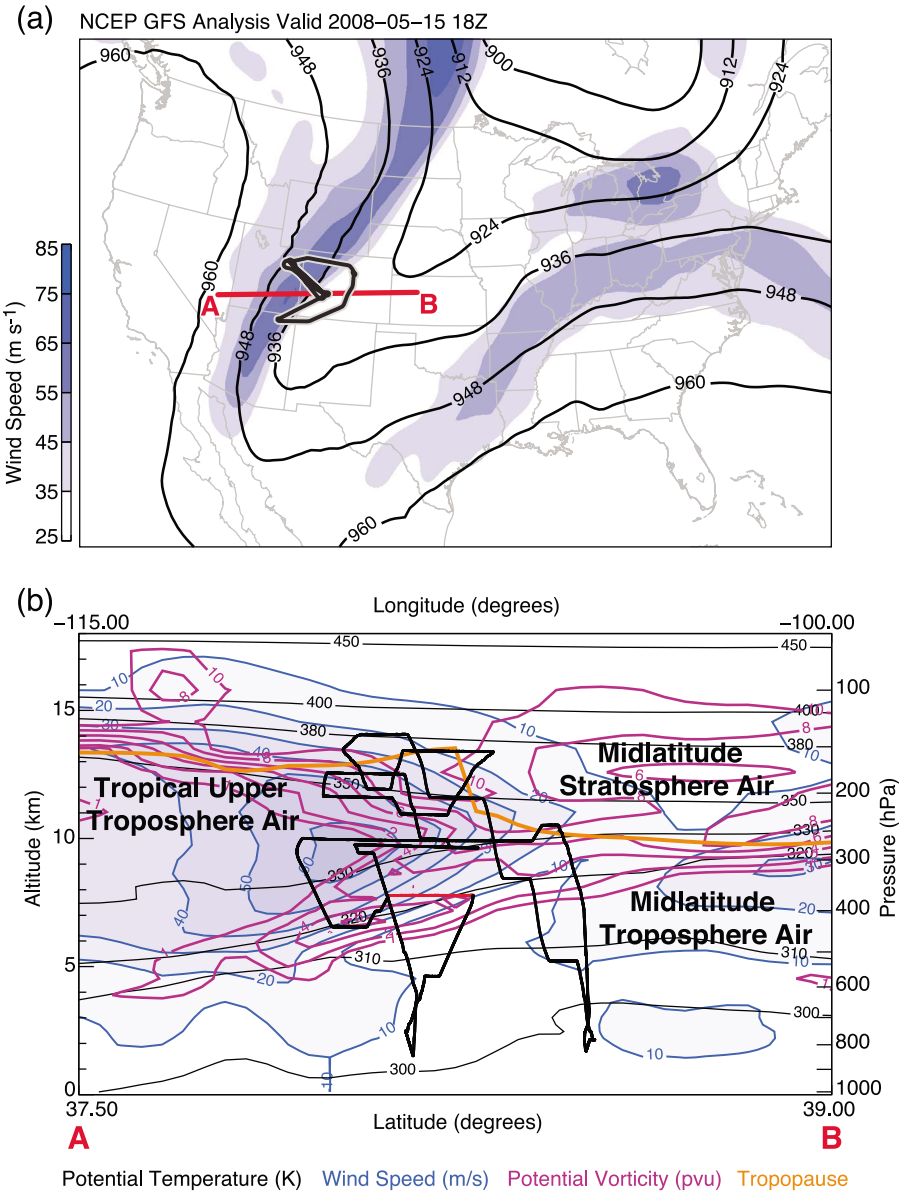

Figure 1. For research flight 12 (RF12): (a) map of GFS analysis 300 hPa wind speed (color-fill) and geopotential height in dm (black lines) valid 15 May 2008 at 18 UTC and (b) vertical cross-section through the observed stratospheric intrusion with potential temperature (black lines), wind speed (color-fill, blue lines), potential vorticity (purple lines), model output lapse-rate tropopause (orange line), and air masses corresponding to the ozone - carbon monoxide scatterplot given in Figure 5a are labeled in black. The vertical section is taken along the red line A–B in the map. The flight track is the black line outlined in gray on the map and the black and red line projected onto the vertical section. Convective injection into the stratospheric intrusion was observed along the red segment of the flight.

events are often found over the ocean storm track regions, which coincide with areas of deep, explosive cyclogenesis [e.g., *Sanders and Gyakum*, 1980; *Roebber*, 1984].

[4] The dynamics of stratospheric intrusions have been discussed widely in the literature, largely in the context of upper-level frontal systems [e.g., *Keyser and Shapiro*, 1986]. These intrusions, characterized by descent below the cyclonic side of an upper-tropospheric jet stream, are the product of a vertical ageostrophic circulation resulting from interactions between horizontal temperature gradients and the geostrophic wind [e.g., *Shapiro*, 1981; *Keyser and Pecnick*, 1985a, 1985b; *Reeder and Keyser*, 1988]. The ageostrophic circulation, as illustrated by *Shapiro* [1981], can be calculated directly for a two-dimensional frontal cross section by using the Sawyer-Eliassen secondary circulation equation [*Sawyer*, 1956; *Eliassen*, 1962]. Large-scale ageostrophic motions from acceleration and curvature effects of the jet stream tend to strengthen the cross-front circulation on the upstream side of a large-amplitude trough and weaken the circulation on the downstream side. The direction and magnitude of the circulation are important for the evolution and large-scale transport of the intrusion.

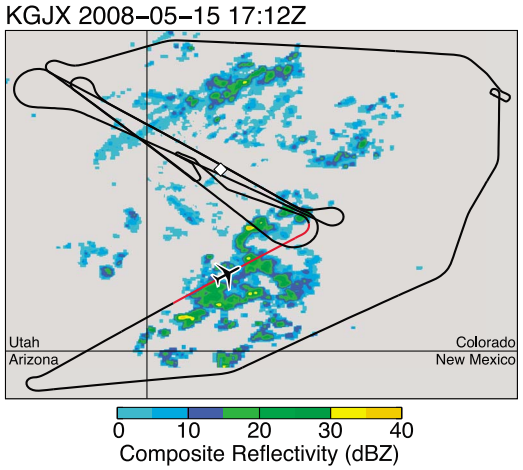

Figure 2. Composite radar reflectivity from the Grand Junction, Colorado (ICAO code KGJX) NEXRAD station on 15 May 2008 at 17:12 UTC. The black and red line is the flight track from research flight 12 (RF12) with red colors denoting the flight segment of convective injection into the observed stratospheric intrusion (as in Figure 1b). The airplane symbol is the aircraft location at the radar analysis time with the nose pointing in the flight direction. The white diamond shows the location of the radar.

[5] There is some indirect evidence for convective injection of tropospheric air into stratospheric intrusions. *Langford and Reid* [1998] use ground based lidar (ozone and aerosol), satellite water vapor images, and radiosonde measurements to suggest that the sudden disappearance of a stratospheric intrusion is the result of moist convective injection. *Reid and Vaughan* [2004] use VHF radar to estimate turbulence, convective injection, and mixing in an observed stratospheric intrusion, but lack in situ measurements to confirm the radar observations. Their analysis also suggests that convective injection in stratospheric intrusions is rare, at least in their radar dataset over Aberystwyth, UK (1 in 17 cases of observed turbulence). The turbulent mixing observed during the convective event from *Reid and Vaughan* [2004] was comparable to the strongest shear turbulence observed. *Cooper et al.* [2005] suggest that variability in ozone and relative humidity below an observed stratospheric intrusion over Hawaii is the result of convective injection into the intrusion. The authors use aircraft data and infrared satellite brightness temperature to associate the observed variability with coincident convection.

[6] A considerable amount of attention has been given to the occurrence of convection that overshoots the lapse-rate tropopause [e.g., *Poulida et al.*, 1996; *Fischer et al.*, 2003; *Wang*, 2003; *Hegglin et al.*, 2004; *Ray et al.*, 2004; *Setvák et al.*, 2008; *Bedka et al.*, 2009; *Pan and Munchak*, 2011]. Although the chemical impacts of overshooting convection and convective injection into stratospheric intrusions may be comparable (both mix tropospheric boundary layer and stratospheric air), they occur under significantly different dynamical conditions. The boundary between a descending stratospheric intrusion and tropospheric air, as identified by potential vorticity and trace constituents, is often several kilometers below the lapse-rate tropopause as defined by the World Meteorological Organization (WMO) definition [*World Meteorological Organization*, 1957]. This is especially true in model analyses, where the vertical resolution may not be sufficient to resolve the stability structure [e.g., *Homeyer et al.*, 2010]. Much of the air in a stratospheric intrusion can return to the stratosphere, but convective injection into stratospheric intrusions may not be identified correctly as troposphere to stratosphere transport because the top of the convection lies below the lapse-rate tropopause. To put this another way, in the vicinity of stratospheric intrusions the lapse-rate tropopause may not be a good indicator of the boundary between tropospheric and stratospheric air.

[7] In this study, we present direct aircraft observations of convection penetrating into two stratospheric intrusions observed during the Stratosphere-Troposphere Analyses of Regional Transport 2008 (START08) field campaign. The convective injection is identified by using in situ trace gas and microphysical measurements, three-dimensional radar reflectivities, and model analyses from the U.S. National

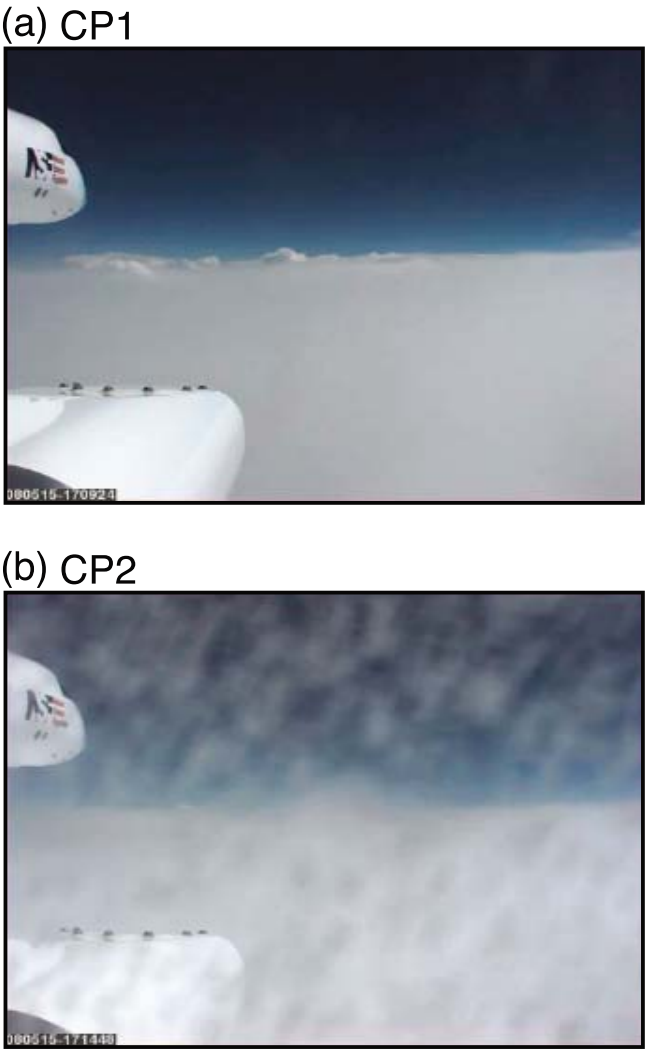

Figure 3. Snapshots from the GV aircraft wing-mounted video camera during convective plumes (a) CP1 and (b) CP2 labeled in Figure 4.

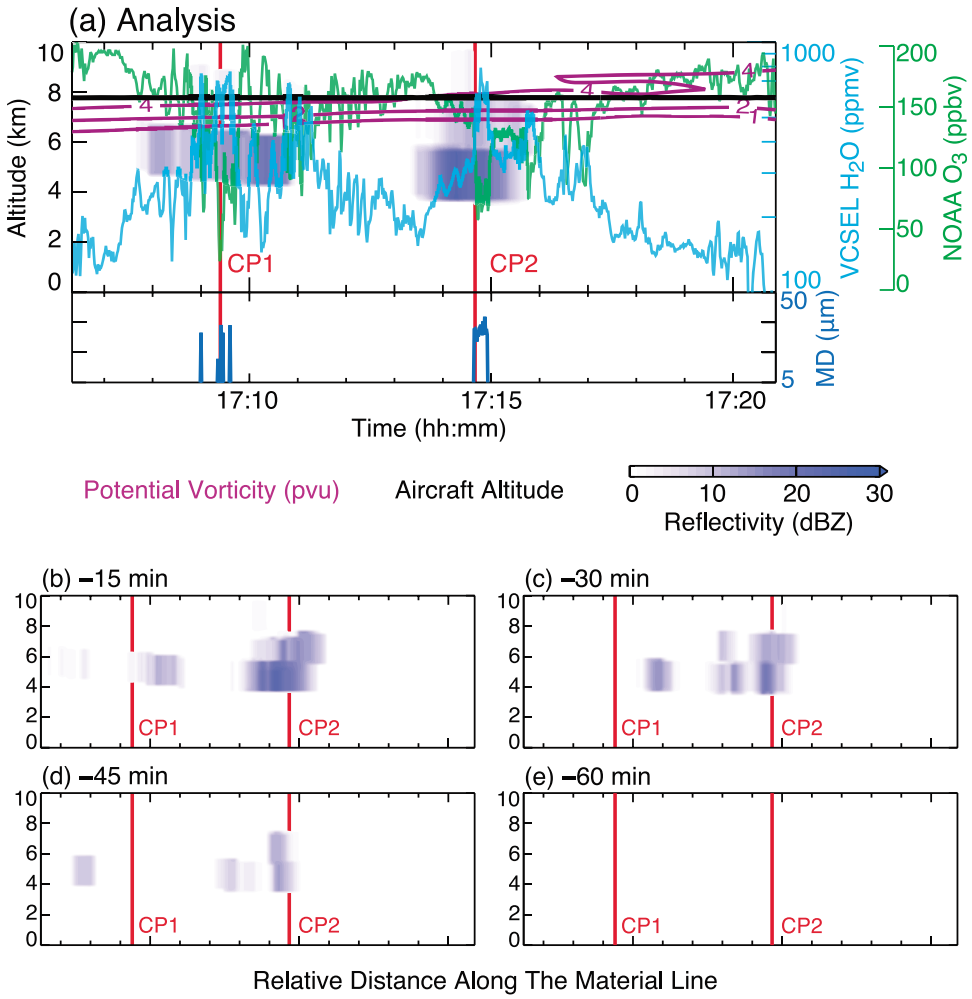

Figure 4. (a) (top) Vertical section of NEXRAD radar reflectivity (blue color-fill) and GFS analysis potential vorticity (purple lines) and in situ measurements of ozone (O_3, green) and water vapor (H_2O, blue) and (bottom) SID-2H mean ice particle diameter (MD, dark blue) along the flight segment of convective injection into the observed stratospheric intrusion from research flight 12 (red portions of the flight track in Figures 1b and 2). The aircraft altitude, which is nearly constant along this flight segment, is the thick black line in the vertical section. Column radar reflectivity along back trajectories from the aircraft analysis times for (b) 15 min, (c) 30 min, (d) 45 min, and (e) 60 min prior. The two convective plumes sampled during RF12 are illustrated by the vertical red lines labeled CP1 and CP2 in each section.

Centers for Environmental Prediction (NCEP) Global Forecast System (GFS). Trace constituents with tropospheric and stratospheric sources are used to identify relationships inherent to convective injection in stratospheric intrusions. We present an additional case study using only model analyses and radar reflectivities to illustrate the relationship between synoptic meteorological conditions and the occurrence of convective injection. In addition, forward trajectories are used to show that two-way exchange of air between the stratosphere and troposphere is possible due to convective injection into tropopause folds.

2. Data and Methods

2.1. START08 Data

[8] During April to June of 2008, the START08 project used the National Science Foundation – National Center for Atmospheric Research (NSF-NCAR) Gulfstream V (GV) aircraft to investigate trace gas distributions in a variety of meteorological situations. The focus was on UTLS transport, but research flights also targeted gravity wave events and convection. For START08 the GV payload was designed to measure atmospheric trace constituents in the UTLS and to study their relationship to transport processes. The GV aircraft flew 18 flights during the project and made extensive measurements in stratospheric intrusions during 4 flights. During Research Flights 12 (RF12) and 6 (RF06), the aircraft flew through and near the tops of convective clouds penetrating into stratospheric intrusions.

[9] The START08 flights extended from the Gulf of Mexico to Canada (~25° to 65°N) and from 85° to ~120°W while reaching a maximum altitude of ~14.3 km. A description of the instrument payload is provided by *Pan et al.* [2010]. Many of the parameters measured by

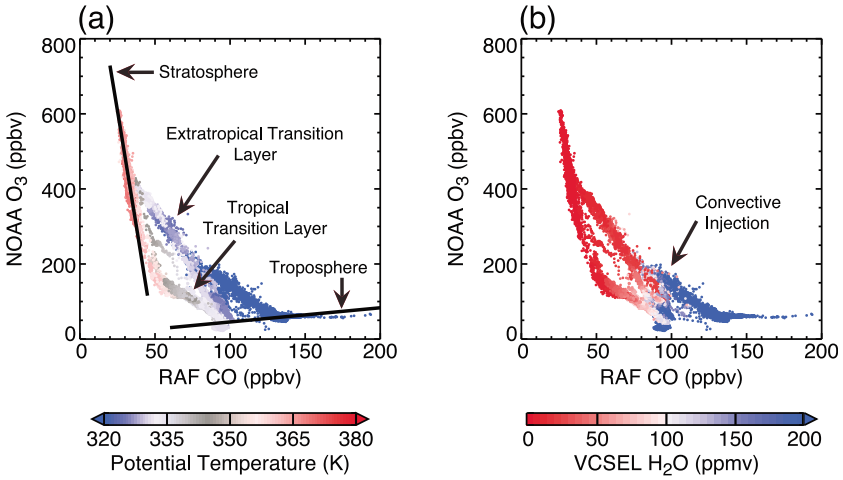

Figure 5. Scatterplot of ozone (O_3) and carbon monoxide (CO) colored by (a) potential temperature and (b) water vapor (H_2O) for research flight 12 (RF12).

instruments on the GV are sampled at 1 Hz, although some trace gas instruments measured less frequently. The spatial resolution of the 1 Hz data is about 200 m at standard cruise speed.

[10] In our analysis we use trace constituents that are useful for diagnosing mixing and large-scale transport. These include ozone (O_3), carbon monoxide (CO), and water vapor (H_2O). Ozone data are from the National Oceanic and Atmospheric Administration (NOAA) dual-beam ultraviolet (UV) absorption ozone photometer [*Proffitt and McLaughlin*, 1983]. The NOAA ozone instrument has a precision of 0.6 ppbv and an accuracy of 3%. Carbon monoxide data are from the NCAR Research Aviation Facility (RAF) vacuum UV resonance fluorescence instrument (similar to that of *Gerbig et al.* [1999]). The RAF carbon monoxide instrument has a precision of 2 ppbv and an accuracy of 5%. Water vapor data are from the vertical cavity surface emitting laser (VCSEL) instrument [*Zondlo et al.*, 2010]. The VCSEL hygrometer has a precision of <3% and an accuracy of 6%. We also use ice particle measurements for cloud identification. Ice particle mean diameter data are from the small ice detector probe (SID-2H). The SID-2H probe infers particle shape by measuring forward scattering intensity at 28 angles around each ice particle using a laser with a wavelength of 532 nm. During START08, the size range measured by the SID-2H probe was ~5–50 μm.

2.2. GFS Data

[11] For dynamical analysis and trajectory calculations, we use the gridded analyses produced by the NCEP Global Data Assimilation System (GDAS) for the high-resolution GFS spectral model. The GFS analyses are assimilated on a Gaussian grid with a longitude-latitude resolution of 0.3125° × ~ 0.3125° (~35 km) and 64 hybrid sigma-pressure levels in the vertical. In the UTLS the vertical resolution is typically 500–1000 m. Analyses are provided daily at 00, 06, 12, and 18 UTC on a 47-level pressure grid.

[12] During RF06 the observed stratospheric intrusion moved rapidly between the available 6-hourly GFS analyses, although the shape of the intrusion did not change much. For example, between the 1 May 2008 18 UTC and 2 May 2008 00 UTC analyses, the tropopause fold moved a distance about equal to the size (or width) of the fold itself. As a result, if simple space-time interpolation is used, the size and magnitude of the fold are underestimated. To provide a more accurate interpolation, we assume that the fold is moving at a constant velocity between analyses, which we estimate subjectively by examination of the two GFS analyses. Interpolating in this moving reference appears to give a more realistic estimate of the structure of the fold. Varying the direction chosen for the moving reference frame by up to ±20 degrees does not significantly change the results. The tropopause fold observed during RF12 was not moving as quickly as the one sampled during RF06, so simple linear interpolation of the GFS analyses in space and time is used.

[13] Trajectory analyses of the observed stratospheric intrusions follow the methods given by *Bowman et al.* [2007]. In this study higher-resolution, three-dimensional GFS analysis wind fields are used with the TRAJ3D trajectory model of *Bowman* [1993] and *Bowman and Carrie* [2002].

2.3. NEXRAD Data

[14] To identify the coverage and vertical extent of convection, we use Next Generation Weather Radar (NEXRAD) program Weather Surveillance Radar – 1988 Doppler (WSR-88D) level II data provided by the National Climatic Data Center (NCDC) [*Crum and Alberty*, 1993]. The level II three-dimensional radar data are available on native spherical grids. Temporal and spatial resolution of the data varies depending on meteorology, operating status, and range from the radar. The typical time between volume scans during precipitation events is 5 to 10 min. For comparison with in situ observations and GFS analyses, radar data are interpolated in space and time, if necessary.

[15] For convenience the NEXRAD level II radar data are transformed to a Cartesian grid. We use the National Center for Atmospheric Research Earth Observing Laboratory (NCAR EOL) REORDER software for grid transformation.

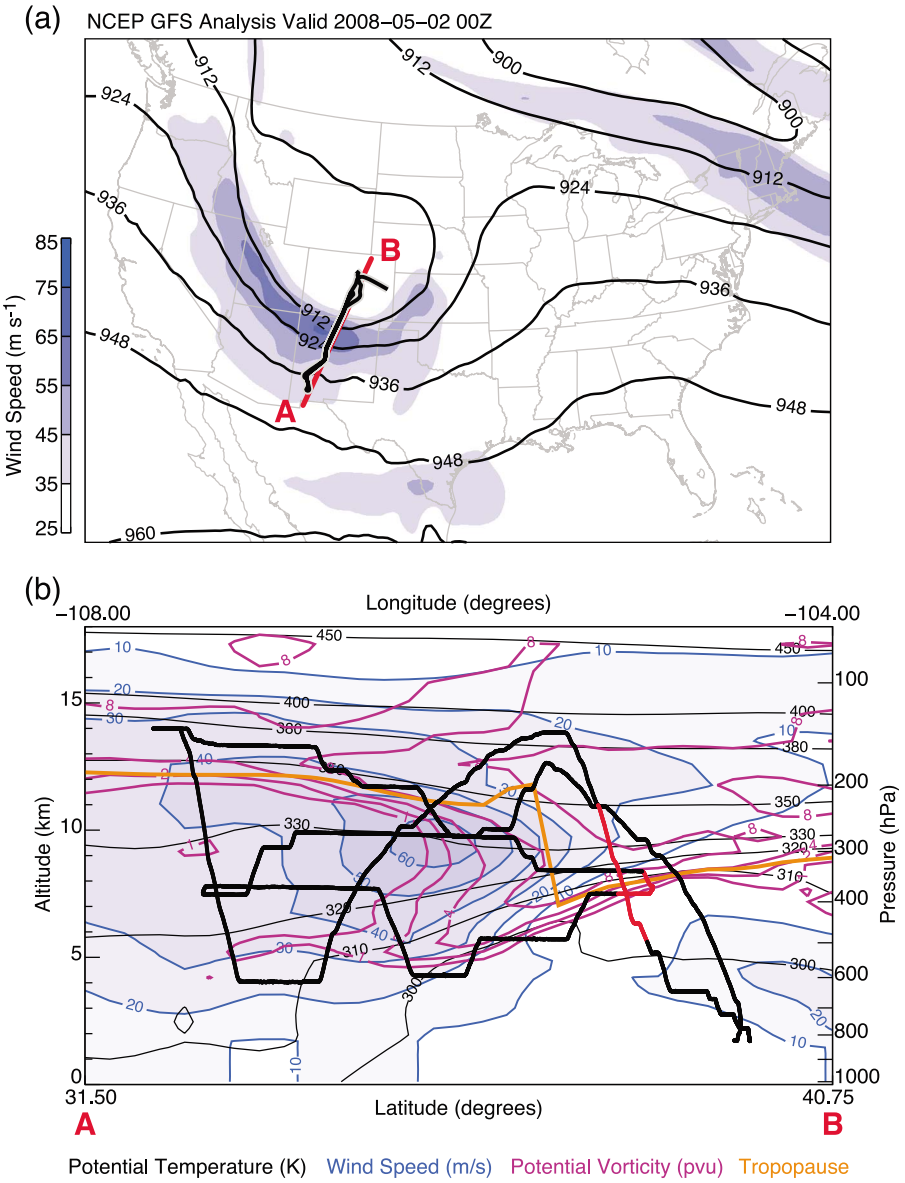

Figure 6. Same as Figure 1 but for research flight 6 (RF06) valid 2 May 2008 at 00 UTC.

The analysis uses a Cressman distance-weighting scheme with a vertical resolution of 250 m and a horizontal resolution of 2 km. For comparison with GFS analyses, we combine observations from several radars by space and time interpolation and averaging, if necessary.

3. Results

3.1. START08 Analysis

3.1.1. Research Flight 12

[16] Research Flight 12 (RF12) provides the clearest observations from START08 of convection penetrating into a stratospheric intrusion. The flight took place on 15 May 2008 from 15:58 to 20:35 UTC. It targeted a stratospheric intrusion descending below the polar jet stream over western Colorado and eastern Utah. Figure 1a shows the 300 hPa wind speed and geopotential height over the continental United States at 18 UTC on 15 May. The flight track is shown on the map by the thick black line with a gray border. The observed stratospheric intrusion, which is shown in the vertical section in Figure 1b, is on the western side of a large-amplitude trough. The section is taken along the red line A–B in Figure 1a. In the section, the intrusion can be seen by the vertically folded structure of the potential vorticity (PV, purple contours). On the anticyclonic side of the jet, the lapse-rate tropopause (orange line) coincides closely with the sharp PV gradient between the troposphere and stratosphere; but on the cyclonic side of the jet, the bottom of the intrusion is between 2 and 7 km below the lapse-rate tropopause. The coordinates of the flight track are shown in black and red and are projected onto the vertical section. During the flight, the aircraft sampled the observed stratospheric intrusion several times and encountered convection within the intrusion during one segment of the flight: the portion of the flight track highlighted in red in Figure 1b.

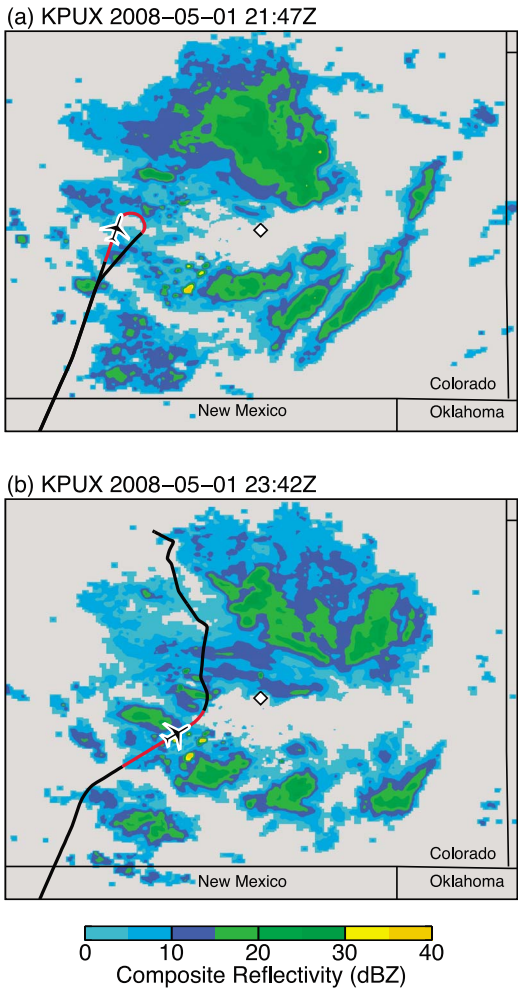

Figure 7. Composite radar reflectivity from the Pueblo, Colorado (ICAO code KPUX) NEXRAD station on 1 May 2008 at (a) 21:47 UTC and (b) 23:42 UTC. The black and red line on each map is the flight track from research flight 6 (RF06) within 30 min of the analysis time. Red colors of each flight track denote flight segments of convective injection into the observed stratospheric intrusion (as in Figure 6b). The airplane symbol in each map is the aircraft location at the radar analysis time with the nose pointing in the flight direction. The white diamonds in each map show the location of the radar.

[17] Scattered convection occurs over western Colorado throughout RF12. Figure 2 shows the composite radar reflectivity from the Grand Junction, Colorado NEXRAD site (KGJX) at 17:12 UTC. This coincides with the flight segment where convection was observed to be penetrating into the stratospheric intrusion. The flight track and location of the aircraft at the radar analysis time are shown in black and the flight segment with observed convective influence in red, with the aircraft nose pointing in the flight direction. The radar reflectivity shows that the aircraft sampled two convective systems along the red flight segment, one just before the radar analysis time shown and the other just after. Hereafter, the first convective system sampled will be referred to as convective plume 1 (CP1) and the second as convective plume 2 (CP2). The presence of active convection at the aircraft altitude is verified by images from the wing-mounted video camera aboard the GV aircraft. Figures 3a and 3b show snapshots from convective plumes CP1 and CP2, respectively. During CP1 the aircraft sampled the top of a convective anvil cloud and during CP2 the aircraft sampled a convective updraft, as can be seen from the ice on the camera lens in Figure 3b.

[18] Data from the GV aircraft show tropospheric levels of trace gases at the times of the encounters with the convective plumes. Figure 4a is a vertical section of radar reflectivity, PV, and aircraft altitude along the red segment of the flight track overlaid with in situ ozone and water vapor measurements. In addition, mean ice particle diameter is plotted directly below the section to identify observations made within clouds. The flight path during this flight segment was straight, level, and within the stratospheric intrusion (black line). The GFS and radar analyses are interpolated in space and time to the flight track. There is no radar information below ~4 km in the vertical section because the altitude of the radar used here, KGJX, is 3.05 km. The encounters with convective plumes CP1 and CP2 (marked by the red vertical lines) are accompanied by peaks in water vapor (500–700 ppmv) and, conversely, valleys in ozone (50–75 ppbv). These features coincide with the radar echoes. Mean ice particle diameters in the convective plumes are ~30–35 μm for both CP1 and CP2. Measurements outside of the convective plumes show higher concentrations of ozone (>150 ppbv) and lower water vapor (<200 ppmv), characteristic of mixed extratropical tropospheric and stratospheric air. The in situ measurements are at altitudes near or above the 4 pvu surface and up to 2 km above the bottom of the stratospheric intrusion. Figures 4b, 4c, 4d and 4e show the recent history of radar reflectivity for the air parcels sampled by the aircraft along this flight segment from backward trajectory calculations. Vertical radar reflectivity sections are plotted along the material line defined by the aircraft path advected backwards in time from the aircraft analysis time to 15, 30, 45 and 60 min earlier, respectively. That is, for a given aircraft measurement, the radar reflectivity in the column containing that air parcel at past times is mapped to the vertical section of aircraft data. For both convective plumes, the magnitude and vertical extent of reflectivity decreases at earlier times, suggesting that the convective influence occurred in the recent past (within the prior 45 min).

[19] Analysis of medium to long-lived trace gas measurements from the GV aircraft illustrates the characteristic source air masses and mixing regimes observed during RF12. In Figure 5a, observations of ozone (O_3) and carbon monoxide (CO) are colored by aircraft potential temperature to identify different mixing regimes. The relationship between O_3 and CO can be used to identify the stratosphere, troposphere, and tropopause transition layer [e.g., *Fischer et al.*, 2000; *Hoor et al.*, 2002; *Pan et al.*, 2004]. The troposphere, stratosphere and transition branches are clearly visible in the aircraft measurements. Following the methods of *Pan et al.* [2004], the stratospheric and tropospheric branches are identified using least-squares polynomial and linear curve fitting, respectively. We use CO < 30 ppbv and O_3 < 70 ppbv to compute the fits for the stratospheric and tropospheric branches. Two characteristic mixing lines

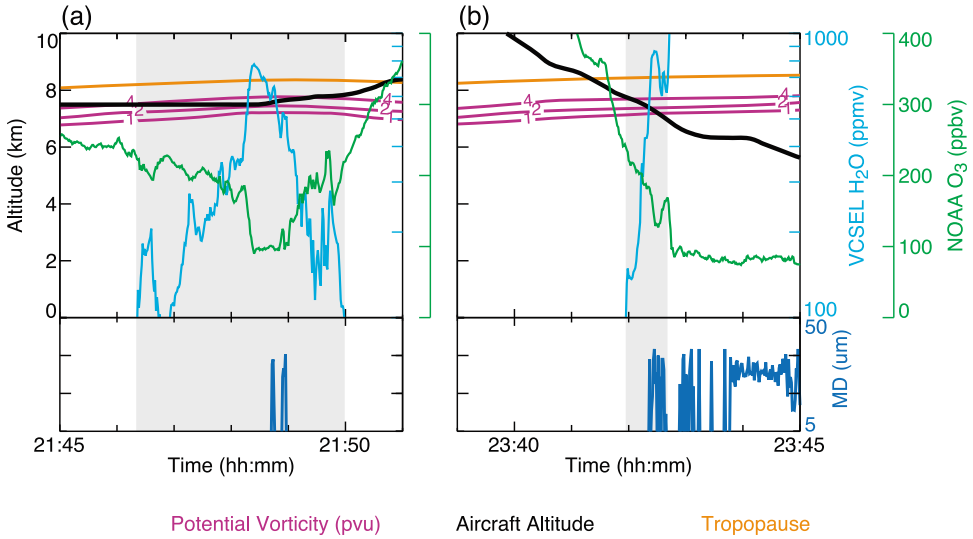

Figure 8. Vertical section of GFS analysis potential vorticity (purple lines) and model output lapse-rate tropopause (orange lines) and in situ measurements of ozone (O_3, green) and water vapor (H_2O, blue) and (bottom) SID-2H mean ice particle diameter (MD, dark blue) along the flight segments of convective injection into the observed stratospheric intrusion from research flight 06 (red portions of the flight track in Figures 6b and 7). The aircraft altitude is the thick black line in each vertical section. The periods of measurement with convective injection characteristics are identified by a gray background.

(tropopause transition layers) are observed during RF12: tropical and extratropical. They can be distinguished by their potential temperatures (labeled in Figure 5a). The aircraft sampled tropical upper tropospheric (UT) air above the stratospheric intrusion on the anticyclonic side of the jet (labeled in the vertical section in Figure 1b). Backward trajectories reveal that this air was in the tropical UT a few days earlier (latitude < 25°N, not shown). The tropical UT air has higher potential temperatures than the extratropical mixing layer, due to its location above the jet core and below the high tropopause on the equatorward side of the jet. This tropical UT air also has much lower O_3 than is typically found in the extratropical transition layer, likely due to convective detrainment of tropical lower troposphere air [e.g., *Folkins et al.*, 1999]. In Figure 5b, mixing by convective injection can be identified by high concentrations of water vapor (>100 ppmv, blue dots) in the extratropical transition layer branch. Additionally, the tropospheric source for convective injection has ~130 ppbv of CO, while the tropospheric source for the remaining observations (no convection, red dots) in the extratropical transition layer has ~100 ppbv.

3.1.2. Research Flight 6

[20] Research Flight 6 (RF06) took place from 1 May 2008 at 19:51 UTC to 2 May 2008 at 00:10 UTC. It targeted a stratospheric intrusion descending below the polar jet stream over southern Colorado and northern New Mexico. The aircraft briefly encountered convection penetrating into the intrusion on two legs of the flight, shown in red in Figure 6b. As in Figure 1, Figures 6a and 6b show 300 hPa wind speed and geopotential height over the continental United States and a vertical section of the GFS analysis at 00 UTC on 2 May, respectively. The flight sampled the observed stratospheric intrusion near the axis of a large-amplitude trough. The section, taken along the red line A–B in Figure 6a, shows that the aircraft sampled the observed stratospheric intrusion several times and at various altitudes. The bottom of the intrusion in this case is up to 5 km below the model lapse-rate tropopause on the cyclonic side of the jet.

[21] The aircraft flew near convective tops during two portions of the flight over southern Colorado. There are large, ongoing areas of shallow convection over south-central and southeastern Colorado throughout the flight. Figures 7a and 7b show maps of the composite radar reflectivity from the Pueblo, Colorado NEXRAD site (KPUX) near the times of each observation of convective injection, 21:47 and 23:42, respectively. The aircraft location at the radar analysis time and flight track (within 30 min of the analysis time) are shown on each map. As in Figure 6b, the red portions of the flight track illustrate measurements during the encounters with convection. The radar reflectivity shows that each observation of convective injection during RF06 was sampled near, but not directly inside, systems penetrating the intrusion.

[22] Trace gas measurements from the aircraft during RF06 show similar characteristics to those observed during RF12. Figures 8a and 8b, similar to Figure 4a, are vertical sections of PV and tropopause altitude overlaid with in situ measurements of ozone, water vapor and mean ice particle diameter and aircraft altitude during each encounter with convective injection. Observations of convective influence are highlighted by a light gray background in each section. During the first encounter (Figure 8a, 21:45–21:51 UTC) the aircraft sampled air with high water vapor (>400 ppmv) and low ozone (~100 ppbv) at PV of 2–4 pvu and below the model lapse-rate tropopause near 21:49 UTC. Observations near the ozone minimum during this flight segment show the

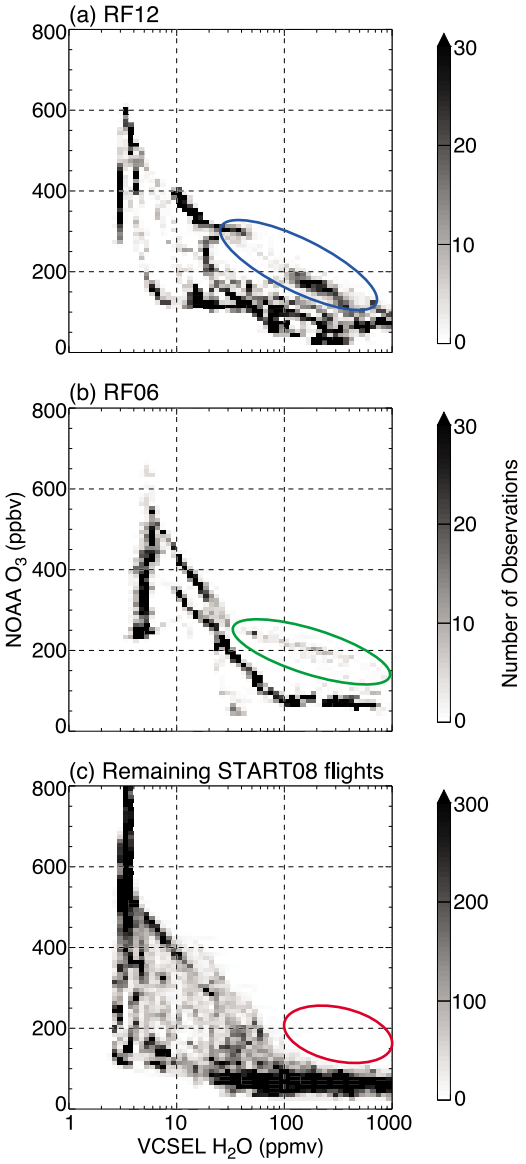

Figure 9. Density plot of ozone (O_3) and water vapor (H_2O) for (a) research flight 12 (RF12), (b) research flight 6 (RF06) and (c) remaining START08 flights. The blue and green ellipses in Figures 9a and 9b encapsulate the observations of convective injection during each flight, respectively. The red ellipse in Figure 9c encapsulates the area where convective injection was observed during research flights 12 and 6. No observations were found in this region during the remaining START08 flights.

presence of convective cloud (large ice particles). In agreement with RF12, measurements outside of the cloud show higher concentrations of ozone (>200 ppbv) and lower water vapor (100–200 ppmv), characteristic of mixed extratropical tropospheric and stratospheric air. During the second encounter with convective injection (Figure 8b, 23:39–23:45 UTC) the aircraft sampled air with similar characteristics at PV up to ~4 pvu while descending through the boundary of the intrusion. The presence of convective cloud during this segment of the flight is observed at PV up to ~2 pvu. Additional analyses of long-lived trace gas measurements for the convective injection observed in RF06 (not shown) are comparable to the results given for RF12 (e.g., Figure 5b).

3.1.3. Trace Gas Relationship

[23] In addition to understanding the source air masses and mixing from measurements of long-lived trace gases, finding a unique signature of convective injection into stratospheric intrusions would be useful for future studies. Figures 9a, 9b, and 9c show density plots of O_3 and water vapor (H_2O) measurements for RF12, RF06, and the remaining START08 flights, respectively. Figure 9c does not include data from research flights 1–3 due to the lack of VCSEL water vapor data. During the remaining thirteen flights, the aircraft did not fly through convection penetrating into a stratospheric intrusion. The measurements of convective injection during RF12 and RF06 are identified by the blue and green ellipses in Figures 9a and 9b, respectively. The observations enclosed by the ellipses for each research flight show lines of mixing between the convectively injected tropospheric air and stratospheric air in the intrusions. The endpoints of these mixing lines identify the trace gas concentrations for each source air mass. In the vertical sections for each flight (Figures 4a and 8), the observations within the convective clouds lie close to the tropospheric ends of the observed mixing lines. The red ellipse in Figure 9c shows the combined area of the blue and green ellipses at $H_2O > 100$ ppmv and shows that for the remaining START08 flights there are few or no observations within the O_3-H_2O space enclosed by the ellipse. These comparisons show that, in all of the measurements made during the START08 project, air from convective injection in stratospheric intrusions is uniquely characterized by $H_2O \geq \sim 100$ ppmv and $O_3 \geq \sim 125$ ppbv.

3.2. Case Study: 11 April 2008

[24] The in situ measurements, model analyses, and radar reflectivities from RF12 and RF06 provide direct evidence of moist convection penetrating into a stratospheric intrusion. Unfortunately, both cases from START08 occurred over high altitude terrain where mean sea level pressure reductions of the surface meteorology can be complicated and often not representative of the responsible synoptic features [e.g., *Allan and Ansell*, 2006]. As we have shown, however, it is possible to use meteorological analyses and radar data to identify and analyze this type of event. In this section, we use GFS analyses and NEXRAD radar data to carry out an additional case study of convective injection in a stratospheric intrusion over the great plains of the continental United States. This example will help develop a better understanding of the relationship between the synoptic-scale meteorology and occurrence of convective injection.

[25] On 11 April 2008 a midlatitude cyclone and associated frontal system was propagating south and east over the great plains of the continental United States. This frontal system was associated with a deep stratospheric intrusion descending along the eastern side of a large-amplitude upper-tropospheric trough. Figure 10a shows mean sea level pressure from the GFS analysis and the National Weather Service (NWS) Hydrometeorological Prediction Center (HPC) surface frontal analysis for 11 April at 00 UTC. The

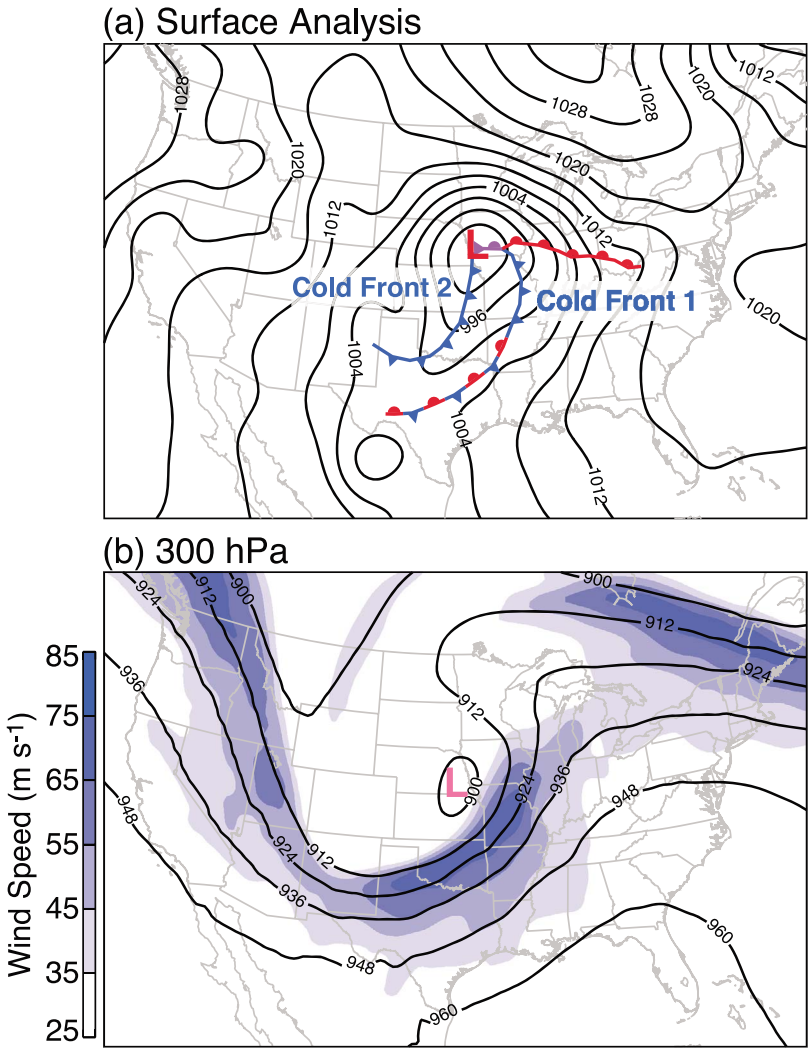

Figure 10. For 11 April 2008 at 00 UTC, maps of (a) GFS mean sea level pressure in hPa (black lines) and National Weather Service Hydrometeorological Prediction Center frontal analysis and (b) GFS 300 hPa wind speed (color-fill) and geopotential height in dm (black lines). In Figure 10a, the location of the surface low (cyclone) is denoted by a large red "L". In Figure 10b, the location of the 300 hPa low (cyclone) is denoted by a large magenta "L".

center of the surface cyclone (large red "L") is located near the Nebraska-Iowa border at the analysis time. There are two surface cold fronts present: the front farther east (cold front 1) is along the leading edge of the deep stratospheric intrusion while the other (cold front 2), lies behind. Cold front 1 has a weak temperature (and moisture) gradient (not shown), which is indicated somewhat by its stationary character in southern Arkansas and Central Texas. Cold front 2, behind the intrusion,has a strong temperature gradient and a classic pressure "kink" along the frontal boundary. These thermal relationships reverse at upper levels, where the temperature gradient for cold front 1 is strong (not shown). Figure 10b shows wind speed and geopotential height at 300 hPa for 11 April at 00 UTC. The upper-level trough and associated cyclone center (large magenta "L") are nearly aligned with the surface cyclone. The upper-level cyclone center is slightly west and south of the observed surface cyclone. For clarity, the remaining analyses are shown for the same analysis time as Figure 10.

[26] The depth of the 11 April stratospheric intrusion is shown in the map in Figure 11a as the *lowest* altitude of the 2 pvu potential vorticity surface. Areas where the 2 pvu surface is folded (and the altitude is multivalued) are colored in blue. Areas where the 2 pvu altitudes are less than 6.5 km are outlined by the thick black line. The location of the surface cyclone center is denoted by the large red "L" (as in Figure 10a). A vertical section of PV, wind speed, the lapse-rate tropopause and NEXRAD radar reflectivity taken along the line A–B is shown in Figure 12. In Figure 11a, the areas where the intrusion is closest to the surface are often in regions where the 2 pvu surface is folded, characteristic of descent below the cyclonic side of the upper-tropospheric jet stream. The folded structure of PV can be clearly seen in the vertical section, with the 2 pvu

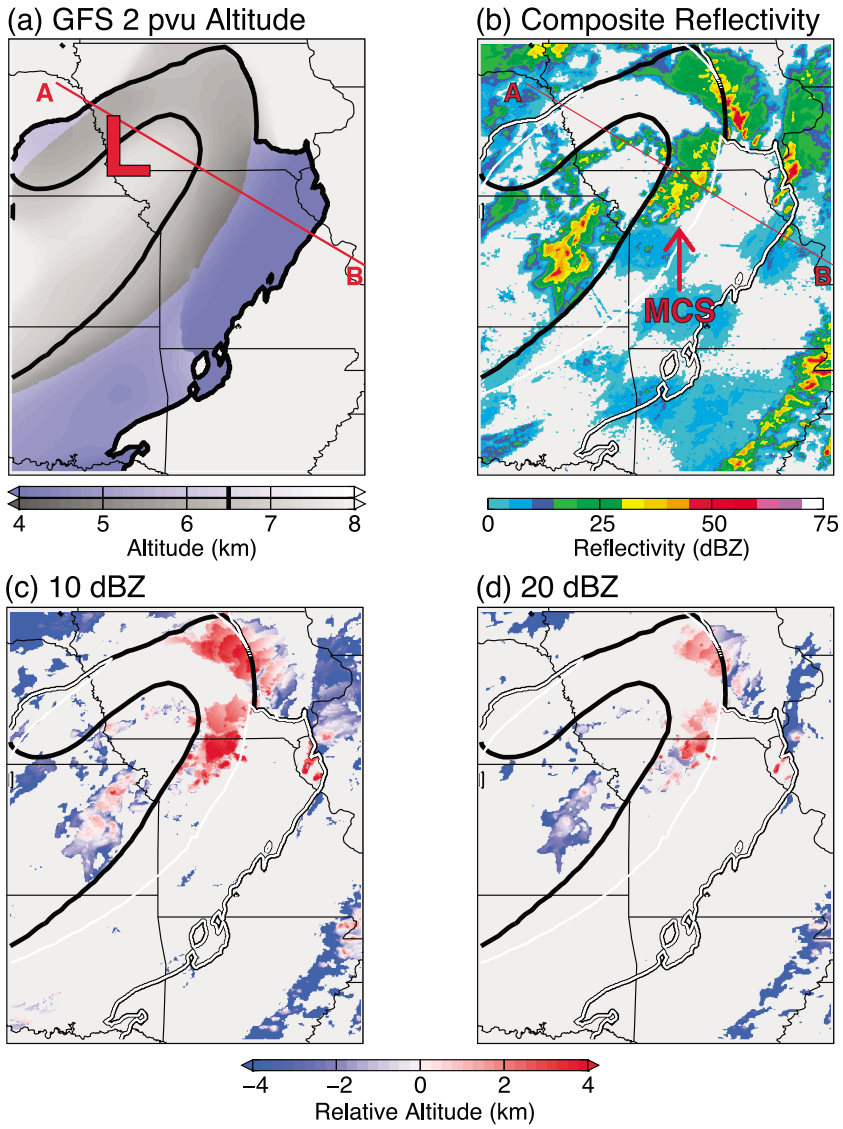

Figure 11. For 11 April 2008 at 00 UTC, maps of (a) altitude of the 2 pvu surface of GFS analysis potential vorticity, (b) NEXRAD composite radar reflectivity, (c) the maximum altitude of the 10 dBZ reflectivity surface relative to the altitude of the 2 pvu surface and (d) as in Figure 11c, but for 20 dBZ. In each map, the 6.5 km altitude contour of the 2 pvu surface is shown by the thick black line. In Figure 11a, the location of the surface low (cyclone) is denoted by a large red "L" and areas where the 2 pvu surface is multivalued (i.e., folded) are colored in blue. In Figures 11b–11d, areas where the 2 pvu surface is multivalued are shown by the thick white lines. In Figures 11a and 11b, the location of the vertical section in Figure 12 is given by the thick red line.

surface up to 7 km below the lowest identifiable lapse-rate tropopause (Figure 12). The analyzed lapse-rate tropopause in this case may be misidentified as the secondary tropopause near the jet stream as illustrated by the large jump from 10 to 17 km in the middle of the section [e.g., *Homeyer et al.*, 2010]. In Figure 11b, the composite radar reflectivity is displayed along with the boundary of the deepest part of the fold (as in Figure 11a) with areas where the 2 pvu surface is folded outlined by a thick white line. There are several mesoscale convective systems (MCSs) and scattered convective cells throughout the domain. The vertical section A–B slices through one of the MCSs in an area where the stratospheric intrusion is deep, but not folded. In Figure 12 the radar reflectivity shows that the MCS reaches altitudes up to ∼10 km. At this level, which is as much as 5 km above the bottom of the intrusion, PV is >4 pvu. To measure the depth of penetration of the convection into the fold, the maximum altitudes of the 10 dBZ and 20 dBZ radar reflectivity surfaces relative to the 2 pvu surface are shown in Figures 11c and 11d, respectively. Red colors indicate locations where convection penetrates through the 2 pvu surface. For reference, the boundaries of the fold are shown as in Figure 11b. The highest convective injection into the intrusion is observed for two large MCSs

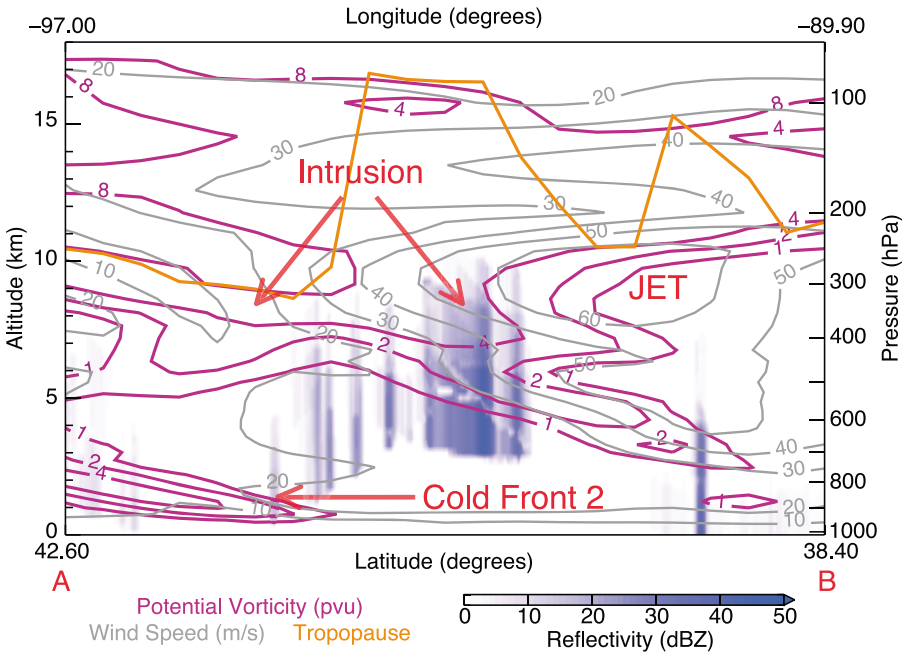

Figure 12. For 11 April 2008 at 00 UTC, a vertical section of GFS potential vorticity (purple lines), wind speed (gray lines) and model output lapse-rate tropopause (orange line) and NEXRAD radar reflectivity (color-fill). The location of the section is shown by the thick red line in Figures 11a and 11b.

in central Iowa and Missouri in areas where the intrusion is deep, but not folded. There are also a few convective cells in western Illinois along the leading edge of the intrusion with tops well above the bottom of the intrusion. The intrusion near these convective cells, however, is folded and the mass of stratospheric air mixed with tropospheric air by the convection is limited compared to the deep convection in areas where the intrusion is not folded. Some convection does penetrate the 2 pvu surface away from the fold where it lies at higher altitude and near the lapse-rate tropopause (e.g., northeastern Arkansas). The depth of injection in those areas, however, is significantly less than where-convection penetrates into the intrusion.

3.3. Trajectory Analysis

[27] One question of importance is whether tropospheric air injected into the fold by convection is simply returned to the troposphere by the descending intrusion, or whether it mixes with air that remains in the stratosphere. To address this question we compute 5-day forward trajectories for the convective injection events from the three case studies. For a typical stratospheric intrusion length scale of 3000 km and a wind speed of 30 m s^{-1}, the timescale for an air parcel to travel the length of an intrusion is 10^5 seconds (~1 day). The life cycle of a stratospheric intrusion, however, can be greater than 4 days. Therefore, a timescale of 5 days is appropriate for the identification of the transport direction of stratospheric air within the fold at the analysis time. It is important to emphasize that these trajectories are driven by the large-scale winds from the GFS analyses and do not include vertical transport by the convection. Rather, the trajectories show the large-scale transport of the convectively influenced air mass.

[28] Figures 13a, 13b and 13c show vertical sections of GFS analyses, NEXRAD radar reflectivity ≥ 1 dBZ, and the destination layers for air parcels initialized along the vertical sections for each case. The section for RF12 (Figure 13a) is taken parallel to the flight segment where convective injection is observed. Radar reflectivities for RF12 are from the analysis time shown in Figure 2. The section for RF06 (Figure 13b) is at the same coordinates as that in Figure 6b and is taken parallel to the flight track and near the observations of convective injection. Radar reflectivities for RF06 are given as the maximum reflectivity of the two analysis times shown in Figure 7. The scattered radar reflectivity features seen above the lapse-rate tropopause in this case are all <5 dBZ and are identified as ground clutter (beam sidelobe contamination) from the mountains west of KPUX. For the NEXRAD radar beam, sidelobe contamination peaks at −29 dB, which is ~3 degrees from the beam center in all directions. The mountains west of KPUX are at elevations up to ~3 km above the altitude of the radar. Under typical atmospheric refraction of the radar beam, sidelobe contamination is possible up to scan elevations of ~6 degrees or altitudes of 9–13 km at the ranges from KPUX in the vertical section for RF06. The section for the 11 April case study (Figure 13c) is the same as that in Figure 12. For each section, the gray color-filled areas indicate stratospheric air that was transported into the troposphere, defined as forward trajectory particles with PV ≥ 1 pvu at the analysis time and altitude below the GFS lapse-rate tropopause 5 days later. Due to column stretching and consequent changes in the static stability, the bottom of a stratospheric intrusion may lie several kilometers below the lapse-rate tropopause. Depending on the subsequent Lagrangian history, however,

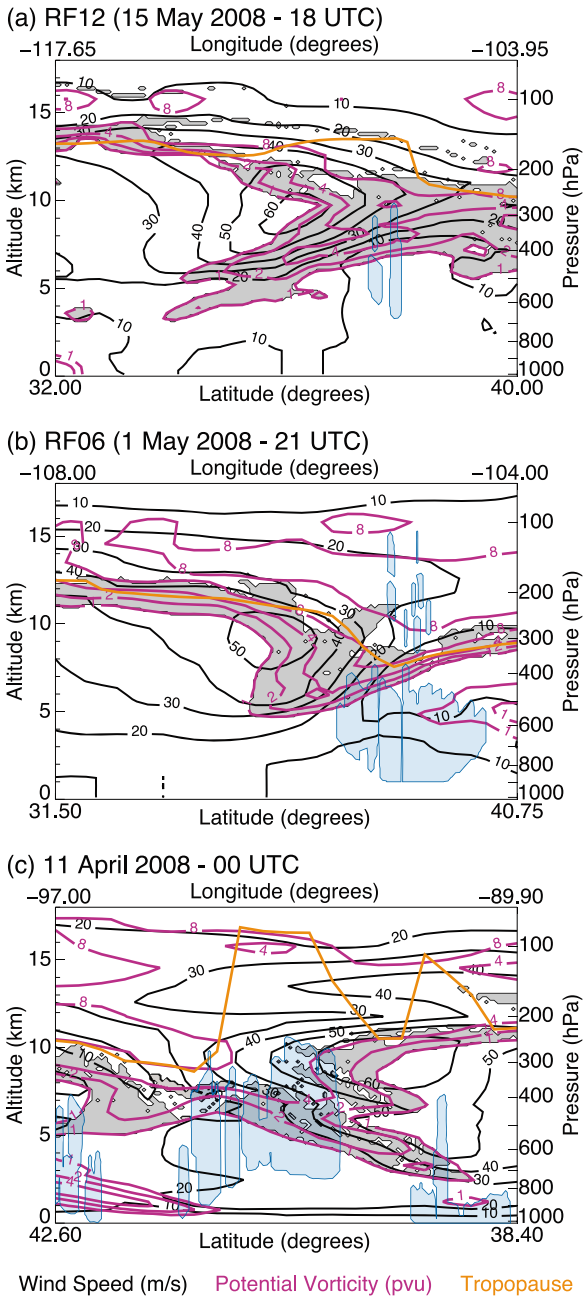

Figure 13. Vertical sections of GFS analysis potential vorticity (PV, purple lines), wind speed (black lines) and model output lapse-rate tropopause (orange lines) and NEXRAD radar reflectivity ≥ 1 dBZ (blue color-fill) for (a) research flight 12 (RF12) parallel to the flight segment of convective injection, (b) research flight 6 (RF06) and (c) the 11 April 2008 case study. The gray color-filled areas indicate air with a stratospheric component that was transported into the troposphere, defined as forward trajectory particles with PV ≥ 1 pvu at the analysis time and at altitudes below the GFS lapse-rate tropopause 5 days later.

the air in the intrusion may remain in the stratosphere or be irreversibly transported into the troposphere.

[29] For RF12, the stratospheric intrusion and much of the lower stratospheric air on the cyclonic side of and below the altitude of the polar jet maximum moves into the troposphere. For RF06, most of the stratospheric intrusion air mass up to and within ∼1 km of the analyzed lapse-rate tropopause is transported into the troposphere. For the 11 April case, the air transported into the troposphere is largely limited to that lying near the boundary of the stratospheric intrusion (PV < 4 pvu). For both START08 research flights, the trajectories show that the tropospheric air injected into the stratosphere by convection returns to the troposphere within a few days. For the 11 April case, much of the convectively influenced air mass at high PV (>4 pvu) remains in the stratosphere (i.e., no gray color-filling). This relationship is clearly shown in the higher altitudes of the MCS (middle of Figure 13c).

[30] It is important to note that the convective injection events for the START08 flights and the 11 April case study occur on opposite sides of their associated upper-level trough axes. For RF12 and RF06, the injection is observed on the upstream side of the upper-level trough, where curvature effects of the wind reinforce the cross-jet ageostrophic circulation that facilitates stratospheric intrusions and descent on the cyclonic side of the jet (see Section 1). For the 11 April case study, convective injection is observed on the downstream side of the upper-level trough, where curvature effects weaken the descent in the fold. These differences in the ageostrophic circulation may be important in determining the primary direction of STE.

4. Summary and Discussion

[31] Aircraft observations from START08 provide the first direct, in situ measurements of convective injection into a stratospheric intrusion. Because the lapse-rate tropopause does not coincide with the bottom of descending stratospheric intrusions, this would not normally be identified as overshooting convection penetrating into the stratosphere. During RF12, the peaks and valleys in trace gas and microphysical data coincide exactly with passage through convective cloud tops, as evidenced by the wing camera imagery from the GV aircraft (Figure 3). Radar reflectivities and trace gas measurements also agree well, demonstrating significant convective influence within the observed intrusion. Similar results are presented for RF06, which sampled convectively injected air near, but not through, the tops of active convection. Convection is observed at altitudes up to 3 km above the bottom of the intrusion during RF12 and up to 2 km above the bottom of the intrusion during RF06 (Figure 13). The convectively injected air masses observed during START08 have characteristics of a mixture of stratospheric and lower-tropospheric or boundary layer air and can be uniquely characterized by $H_2O \geq \sim 100$ ppmv and $O_3 \geq \sim 125$ ppbv. A wider range of samples will be required to establish that this trace gas relationship is unique to convectively injected air in all circumstances.

[32] The 11 April 2008 case study illustrates the potential extent of convective mixing associated with a tropopause fold. The observations show that convective injection can be deep, reaching altitudes more than 5 km above the bottom of the intrusion and PV surfaces >4 pvu, near the altitude of the polar jet maximum. Based on these cases and previous research, we propose a conceptual model of the synoptic conditions conducive to convective injection in stratospheric

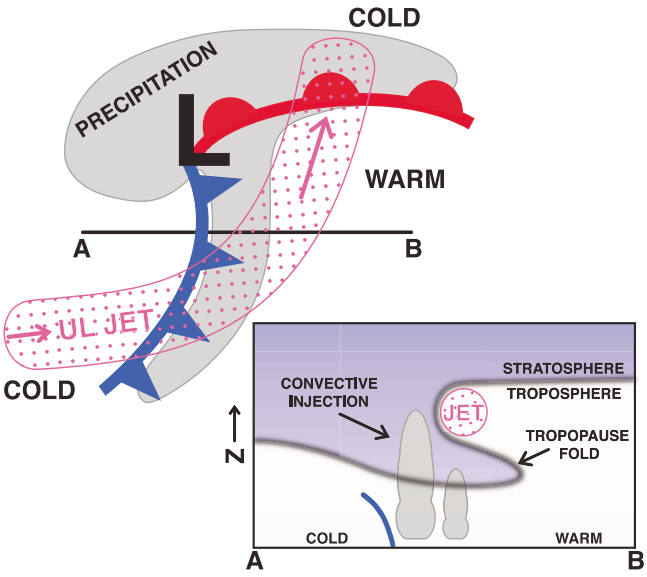

Figure 14. Conceptual model of the synoptic meteorological conditions conducive to convective injection in stratospheric intrusions. The upper left is a representation of the associated surface and upper-level meteorological conditions. The vertical section, along line A–B, shows the stratospheric intrusion ahead of the surface cold front (a "split front") and location of convective injection.

intrusions. Figure 14 is a schematic of the surface and upper-level meteorological conditions characteristic of such transport events. In the mature or decaying phase of a midlatitude cyclone, when the upper-level trough catches up with the low-level cyclone, the upper-level polar jet stream can be located above the warm sector of the surface cyclone. Given the existence of a stratospheric intrusion, deep convective injection is most likely along or ahead of the leading edge of the surface cold front. This meteorological condition is well documented and often referred to as a "split front", meaning the surface and upper level fronts (commonly the leading edge of the intrusion) are not continuous with height [e.g., *Newton*, 1963; *Shapiro*, 1982; *Browning and Monk*, 1982]. Because this is a common synoptic situation, it seems likely that convective injection into stratospheric intrusions is a relatively frequent occurrence in midlatitudes. In fact, recent work suggests this meteorological condition may be a consequence of the midlatitude cyclone occlusion process [e.g., *Schultz and Vaughan*, 2011].

[33] It should be noted that the PV analyses shown here do not account for the non-conservative processes associated with the penetrating convection that irreversibly mix tropospheric and stratospheric air. This convective mixing can erode the lower altitude intrusion air mass and effectively elevate the tropopause. The PV analyses do, however, illustrate the bounds of stratospheric influence associated with the observed intrusions. This relationship is shown clearly in Figures 4a and 8.

[34] Downward transport of stratospheric air into the troposphere by tropopause folding has been known and studied for many years. The trajectory analysis for the three cases shows that STE can potentially occur in both directions due to tropopause folding. When deep convective injection occurs, it could have a significant impact on the distribution of chemically and radiatively important trace species in the lower stratosphere. The transport direction, and even the depth of convective injection, maybe dependent on the strength of the cross-jet ageostrophic circulation that facilitates stratospheric intrusions, as suggested by Figure 13 (see also the discussion in Section 1).

[35] The depth of convective injection is greater in the 11 April case study than during START08 RF12 and RF06. The depth and extent of convective injection in a stratospheric intrusion may have a larger impact on the composition of the UTLS than deep convection penetrating a flat tropopause. The frequency of occurrence and seasonality of these events, however, are not well known. In previous studies, convective overshooting of the lapse-rate tropopause is found at altitudes in the lower stratosphere with peak ozone (O_3) concentrations of 150–200 ppbv [e.g., *Poulida et al.*, 1996; *Fischer et al.*, 2003; *Hegglin et al.*, 2004]. The peak ozone concentrations at the altitude of convective injection in the stratospheric intrusions observed during START08 RF12 and RF06 are comparable at ~200 and ~250 ppbv, respectively (Figures 4, 5 and 8). It is also possible that convection penetrates more deeply into stratospheric intrusions due to the lower static stability relative to the unfolded tropopause [e.g., *Shapiro*, 1982; *Griffiths et al.*, 2000]. Recent modeling studies suggest that the contribution of moist convection to stratosphere-to-troposphere transport can be large in midlatitudes, especially over land during the summer [e.g., *Gray*, 2003; *Tang et al.*, 2011]. Therefore, an understanding of the relative contributions of convective injection into stratospheric intrusions and convective overshooting of the lapse-rate tropopause, as well as their seasonality, is important for the accurate determination of STE in the extratropics.

[36] **Acknowledgments.** We acknowledge the START08 project, which was funded by the National Science Foundation, for access to the aircraft data, the NCAR RAF for access to the wing-mounted video camera footage, Ru-Shan Gao at NOAA for access to the NOAA ozone data, Andrew Heymsfield and Aaron Bansemer at NCAR for access to the SID-2H ice particle data, and Teresa Campos at NCAR for access to the RAF carbon monoxide data. We also thank John Nielsen-Gammon and Don Conlee at Texas A&M University for helpful discussions. This research was funded by National Science Foundation grants ATM-072225 and AGS-1016191 to Texas A&M University.

References

Allan, R., and T. Ansell (2006), A new globally complete monthly Historical Gridded Mean Sea Level Pressure dataset (HadSLP2): 1850–2004, *J. Clim.*, *19*, 5816–5842.

Appenzeller, C., and H. C. Davies (1992), Structure of stratospheric intrusions into the troposphere, *Nature*, *358*, 570–572.

Appenzeller, C., H. C. Davies, and W. A. Norton (1996), Fragmentation of stratospheric intrusions, *J. Geophys. Res.*, *101*(D1), 1435–1456.

Bedka, K., J. Brunner, R. Dworak, W. Feltz, J. Otkin, and T. Greenwald (2009), Objective satellite-based detection of overshooting tops using infrared window channel brightness temperature gradients, *J. Appl. Meteorol. Climatol.*, *49*, 181–202, doi:10.1175/2009JAMC2286.1.

Bowman, K. P. (1993), Large-scale isentropic mixing properties of the Antarctic polar vortex from analyzed winds, *J. Geophys. Res.*, *98*(D12), 23,013–23,027.

Bowman, K. P., and G. D. Carrie (2002), The mean-meridional transport circulation of the troposphere in an idealized GCM, *J. Atmos. Sci.*, *59*, 1502–1514.

Bowman, K. P., L. L. Pan, T. Campos, and R. Gao (2007), Observations of fine-scale transport structure in the upper troposphere from the High-performance Instrumented Airborne Platform for Environmental Research, *J. Geophys. Res.*, *112*, D18111, doi:10.1029/2007JD008685.

Browell, E. V., E. F. Danielsen, S. Ismail, G. L. Gregory, and S. M. Beck (1987), Tropopause fold structure determined from airborne lidar in situ measurements, *J. Geophys. Res.*, *92*(D2), 2112–2120.

Browning, K. A., and G. A. Monk (1982), A simple model for the synoptic analysis of cold fronts, *Q. J. R. Meteorol. Soc.*, *108*, 435–452.

Cooper, O., et al. (2004), On the life cycle of a stratospheric intrusion and its dispersion into polluted warm conveyor belts, *J. Geophys. Res.*, *109*, D23S09, doi:10.1029/2003JD004006.

Cooper, O. R., et al. (2005), Direct transport of midlatitude stratospheric ozone into the lower troposphere and marine boundary layer of the tropical Pacific Ocean, *J. Geophys. Res.*, *110*, D23310, doi:10.1029/2005JD005783.

Crum, T. D., and R. L. Alberty (1993), The WSR-88D and the WSR-88D operational support facility, *Bull. Am. Meteorol. Soc.*, *74*(9), 1669–1687.

Danielsen, E. F. (1968), Stratospheric-tropospheric exchange based on radioactivity, ozone and potential vorticity, *J. Atmos. Sci.*, *25*, 502–518.

Danielsen, E. F., R. S. Hipskind, W. L. Starr, J. F. Vedder, S. E. Gaines, D. Kley, and K. K. Kelly (1991), Irreversible transport in the stratosphere by internal waves of short vertical wavelength, *J. Geophys. Res.*, *96*(D9), 17,433–17,452.

Eliassen, A. (1962), On the vertical circulation in frontal zones, *Geofys. Publ.*, *24*, 147–160.

Fischer, H., F. G. Wienhold, P. Hoor, O. Bujok, C. Schiller, P. Siegmund, M. Ambaum, H. A. Scheeren, and J. Lelieveld (2000), Tracer correlations in the northern high latitude lowermost stratosphere: Influence of cross-tropopause mass exchange, *Geophys. Res. Lett.*, *27*(1), 97–100.

Fischer, H., et al. (2003), Deep convective injection of boundary layer air into the lowermost stratosphere at midlatitudes, *Atmos. Chem. Phys.*, *3*(3), 739–745.

Flentje, H., A. Dörnbrack, G. Ehret, A. Fix, C. Kiemle, G. Poberaj, and M. Wirth (2005), Water vapor heterogeneity related to tropopause folds over the North Atlantic revealed by airborne water vapor differential absorption lidar, *J. Geophys. Res.*, *110*, D03115, doi:10.1029/2004JD004957.

Folkins, I., M. Loewenstein, J. Podolske, S. J. Oltmans, and M. Proffitt (1999), A barrier to vertical mixing at 14 km in the tropics: Evidence from ozonesondes and aircraft measurements, *J. Geophys. Res.*, *104*(D18), 22,095–22,102.

Gerbig, C., S. Schmitgen, D. Kley, A. Volz-Thomas, K. Dewey, and D. Haaks (1999), An improved fast-response vacuum-UV resonance fluorescence CO instrument, *J. Geophys. Res.*, *104*(D1), 1699–1704.

Gray, S. L. (2003), A case study of stratosphere to troposphere transport: The role of convective transport and the sensitivity to model resolution, *J. Geophys. Res.*, *108*(D18), 4590, doi:10.1029/2002JD003317.

Griffiths, M., A. J. Thorpe, and K. A. Browning (2000), Convective destabilization by a tropopause fold diagnosed using potential-vorticity inversion, *Q. J. R. Meteorol. Soc.*, *126*, 125–144.

Hegglin, M. I., et al. (2004), Tracing troposphere-to-stratosphere transport above a mid-latitude deep convective system, *Atmos. Chem. Phys.*, *4*(3), 741–756, doi:10.5194/acp-4-741-2004.

Holton, J. R., P. H. Haynes, M. E. McIntyre, A. R. Douglass, and L. Pfister (1995), Stratosphere-troposphere exchange, *Rev. Geophys.*, *33*(4), 403–439.

Homeyer, C. R., K. P. Bowman, and L. L. Pan (2010), Extratropical tropopause transition layer characteristics from high-resolution sounding data, *J. Geophys. Res.*, *115*, D13108, doi:10.1029/2009JD013664.

Hoor, P., H. Fischer, L. Lange, J. Lelieveld, and D. Brunner (2002), Seasonal variations of a mixing layer in the lowermost stratosphere as identified by the CO-O_3 correlation from in situ measurements, *J. Geophys. Res.*, *107*(D5), 4044, doi:10.1029/2000JD000289.

Hoskins, B. J. (1991), Towards a PV-theta view of the general circulation, *Tellus*, *43*, 27–35.

Johnson, W. B., and W. Viezee (1981), Stratospheric ozone in the lower troposphere -I. Presentation and interpretation of aircraft measurements, *Atmos. Environ.*, *15*(7), 1309–1323.

Keyser, D., and M. J. Pecnick (1985a), Diagnosis of ageostropic circulations in a two-dimensional primitive equation model of frontogenesis, *J. Atmos. Sci.*, *42*(12), 1283–1305.

Keyser, D., and M. J. Pecnick (1985b), A two-dimensional primitive equation model of frontogenesis forced by confluence and horizontal shear, *J. Atmos. Sci.*, *42*(12), 1259–1282.

Keyser, D., and M. A. Shapiro (1986), A review of the structure and dynamics of upper-level fronal zones, *Mon. Weather Rev.*, *114*, 452–499.

Lamarque, J.-F., and P. G. Hess (1994), Cross-tropopause mass exchange and potential vorticity budget in a simulated tropopause folding, *J. Atmos. Sci.*, *51*(15), 2246–2269.

Langford, A. O., and S. J. Reid (1998), Dissipation and mixing of a small-scale stratospheric intrusion in the upper troposphere, *J. Geophys. Res.*, *103*(D23), 31,265–31,276.

Newton, C. W. (1963), Dynamics of severe convective storms, *Meteorol. Monogr.*, *5*(27), 33–58.

Olsen, M. A., A. R. Douglass, and M. R. Schoeberl (2002), Estimating downward cross-tropopause ozone flux using column ozone and potential vorticity, *J. Geophys. Res.*, *107*(D22), 4636, doi:10.1029/2001JD002041.

Pan, L. L., and L. A. Munchak (2011), Relationship of cloud top to the tropopause/jet structure from CALIPSO data, *J. Geophys. Res.*, *116*, D12201, doi:10.1029/2010JD015462.

Pan, L. L., W. J. Randel, B. L. Gary, M. J. Mahoney, and E. J. Hintsa (2004), Definitions and sharpness of the extratropical tropopause: A trace gas perspective, *J. Geophys. Res.*, *109*, D23103, doi:10.1029/2004JD004982.

Pan, L. L., et al. (2007), Chemical behavior of the tropopause observed during the stratosphere-troposphere analyses of regional transport experiment, *J. Geophys. Res.*, *112*, D18110, doi:10.1029/2007JD008645.

Pan, L. L., et al. (2010), The Stratosphere-Troposphere Analyses of Regional Transport 2008 experiment, *Bull. Am. Meteorol. Soc.*, *91*, 327–342.

Poulida, O., R. R. Dickerson, and A. Heymsfield (1996), Stratosphere-troposphere exchange in a midlatitude mesoscale convective complex, *J. Geophys. Res.*, *101*(D3), 6823–6836.

Price, J. D., and G. Vaughan (1993), The potential for stratosphere-troposphere exchange in cut-off-low systems, *Q. J. R. Meteorol. Soc.*, *119*, 343–365.

Proffitt, M. H., and R. J. McLaughlin (1983), Fast-response dual-beam UV-absorption ozone photometer suitable for use on stratospheric balloons, *Rev. Sci. Instrum.*, *54*(12), 1719–1728.

Ray, E. A., et al. (2004), Evidence of the effect of summertime midlatitude convection on the subtropical lower stratosphere from CRYSTAL-FACE tracer measurements, *J. Geophys. Res.*, *109*, D18304, doi:10.1029/2004JD004655.

Reed, R. J. (1955), A study of a characteristic type of upper-level frontogenesis, *J. Meteorol.*, *12*, 226–237.

Reeder, M. J., and D. Keyser (1988), Balanced and unbalanced upper-level frontogenesis, *J. Atmos. Sci.*, *45*(22), 3366–3386.

Reid, H. J., and G. Vaughan (2004), Convective mixing in a tropopause fold, *Q. J. R. Meteorol. Soc.*, *130*, 1195–1212.

Roebber, P. J. (1984), Statistical analysis and updated climatology of explosive cyclones, *Mon. Weather Rev.*, *112*, 1577–1589.

Sanders, F., and J. R. Gyakum (1980), Synoptic-dynamic climatology of the "bomb," *Mon. Weather Rev.*, *108*, 1589–1606.

Sawyer, J. S. (1956), The vertical circulation at meteorological fronts and its relation to frontogenesis, *Proc. R. Soc. A*, *234*, 346–362.

Schultz, D. M., and G. Vaughan (2011), Occluded fronts and the occlusion process: A fresh look at conventional wisdom, *Bull. Am. Meteorol. Soc.*, *92*(4), 443–466, doi:10.1175/2010BAMS3057.1.

Seo, K.-H., and K. P. Bowman (2001), A climatology of isentropic cross-tropopause exchange, *J. Geophys. Res.*, *106*(D22), 28,159–28,172.

Setvák, M., D. T. Lindsey, R. M. Rabin, P. K. Wang, and A. Demeterová (2008), Indication of water vapor transport into the lower stratosphere above midlatitude convective storms: Meteosat Second Generation satellite observations and radiative transfer model simulations, *Atmos. Res.*, *89*, 170–180, doi:10.1016/j.atmosres.2007.11.031.

Shapiro, M. A. (1976), The role of turbulent heat flux in the generation of potential vorticity in the vicinity of upper-level jet stream systems, *Mon. Weather Rev.*, *104*, 892–906.

Shapiro, M. A. (1978), Further evidence of the mesoscale and turbulent structure of upper level jet stream-frontal zone systems, *Mon. Weather Rev.*, *106*, 1100–1111.

Shapiro, M. A. (1980), Turbulent mixing within tropopause folds as a mechanism for the exchange of chemical constituents between the stratosphere and troposphere, *J. Atmos. Sci.*, *37*, 994–1004.

Shapiro, M. A. (1981), Frontogenesis and geostrophically forced secondary circulations in the vicinity of jet stream-frontal zone systems, *J. Atmos. Sci.*, *38*, 954–973.

Shapiro, M. A. (1982), Mesoscale weather systems of the central United States, in *The National STORM Program: Scientific and Technological Bases and Major Objectives*, *Tech. Rep. 3.1–3.77*, edited by R. A. Anthes, Univ. Corp. for Atmos. Res., Boulder, Colo.

Shapiro, M. A., T. Hampel, and A. J. Krueger (1987), The arctic tropopause fold, *Mon. Weather Rev.*, *115*, 444–454.

Sprenger, M., and H. Wernli (2003), A northern hemispheric climatology of cross-tropopause exchange for the ERA15 time period (1979–1993), *J. Geophys. Res.*, *108*(D12), 8521, doi:10.1029/2002JD002636.

Sprenger, M., M. C. Maspoli, and H. Wernli (2003), Tropopause folds and cross-tropopause exchange: A global investigation based upon ECMWF

analyses for the time period March 2000 to February 2001, *J. Geophys. Res.*, *108*(D12), 8518, doi:10.1029/2002JD002587.

Stohl, A., H. Wernli, P. James, M. Bourqui, C. Forster, M. A. Liniger, P. Seibert, and M. Sprenger (2003), A new perspective of stratosphere-troposphere exchange, *Bull. Am. Meteorol. Soc.*, *84*(11), 1565–1573.

Tang, Q., M. J. Prather, and J. Hsu (2011), Stratosphere-troposphere exchange ozone flux related to deep convection, *Geophys. Res. Lett.*, *38*, L03806, doi:10.1029/2010GL046039.

Wang, P. K. (2003), Moisture plumes above thunderstorm anvils and their contributions to cross-tropopause transport of water vapor in midlatitudes, *J. Geophys. Res.*, *108*(D6), 4194, doi:10.1029/2002JD002581.

Waugh, D. W., and L. M. Polvani (2000), Climatology of intrusions into the tropical upper troposphere, *Geophys. Res. Lett.*, *27*(23), 3857–3860.

Wernli, H., and M. Bourqui (2002), A Lagrangian "1-year climatology" of (deep) cross-tropopause exchange in the extratropical Northern Hemisphere, *J. Geophys. Res.*, *107*(D2), 4021, doi:10.1029/2001JD000812.

World Meteorological Organization (1957), Meteorology—A three-dimensional science: Second session of the commission for aerology, *World Meteorol. Org. Bull.*, *4*, 134–138.

Zondlo, M. A., M. E. Paige, S. M. Massick, and J. A. Silver (2010), Vertical cavity laser hygrometer for the National Science Foundation Gulfstream-V aircraft, *J. Geophys. Res.*, *115*, D20309, doi:10.1029/2010JD014445.

K. P. Bowman and C. R. Homeyer, Department of Atmospheric Sciences, Texas A&M University, 3150 TAMU, College Station, TX 77843-3150, USA. (k-bowman@tamu.edu; chomeyer@tamu.edu)

J. F. Bresch and L. L. Pan, National Center for Atmospheric Research, PO Box 3000, Boulder, CO 80307–3000, USA. (bresch@ucar.edu; liwen@ucar.edu)

M. A. Zondlo, Department of Civil and Environmental Engineering, Princeton University, Engineering Quad, C-330, Princeton, NJ 08544, USA. (mzondlo@princeton.edu)